Highly birefringent octagonal photonic crystal fibers with two zero-dispersion wavelengths

Changming Xia (夏长明)[1*], Guiyao Zhou (周桂耀)[1,2], Ying Han (韩 颖) [1], and Lantian Hou (侯蓝田)[1]

[1]*State Key Laboratory of Metastable Materials Science and Technology, Yanshan University, Qinhuangdao 066004, China*

[2]*School of Information and Optoelectronic Science and Engineering, South China Normal University, Guangzhou 510006, China*

[*]*Corresponding author: xiacmm@126.com*

Received March 14, 2011; accepted May 9, 2011; posted online August 5, 2011

A new highly birefringent octagonal photonic crystal fiber (Hi-Bi OPCF) with a rectangular array of four elliptical airholes in the fiber core region is proposed and analyzed using the full-vector finite element method with anisotropic perfect match layer absorbing boundaries. Numerical results show that the phase birefringence of the photonic crystal fiber (PCF) reaches 3.43×10^{-2} at the wavelength of 1 550 nm. Moreover, two zero-dispersion wavelengths are achieved in the visible and near infrared wavelength regions for one polarization state but not in the other.

OCIS codes: 060.2400, 060.2280.
doi: 10.3788/COL201109.100609.

Photonic crystal fibers (PCFs)[1−3] have a wavelength-scale periodic silica-air microstructure around the core along their length, providing much more degrees of freedom for tailoring the properties of PCF, such as chromatic dispersion[4,5], confinement loss[6], nonlinear[7], and birefringence. As a result, it is also possible to fabricate a highly birefringent PCF by introducing suitable airholes in cladding[8,9]. Recently, great attention has been devoted to the enhancement of birefringence of PCF[10−13], because the highly birefringent polarization maintaining PCFs have been widely used in the fiber communication systems and sensing applications[14,15]. Some highly birefringent hexagonal PCFs have been proposed by introducing an asymmetric structure[12,13,16]. An *et al.*[17] reported an ultrahigh birefringent hexagonal PCF with ultralow confinement loss using four airholes in the core, An ultrahigh mode birefringence is realized with a mode birefringence of up to 10^{-2}. Moreover, hexagonal photonic bandgap fibers (PBGFs) with asymmetric air cores have also been suggested in high birefringence[18]. However, there are few reports for highly birefringent octagonal PCFs (OPCFs). OPCFs have isosceles triangular unit lattices with a vertex angle of 45°; for the same numbers of air-hole rings in cladding, OPCFs have more airholes than the conventional hexagonal PCF, resulting in an increase in the air-filling ratios[19,20]. Due to these properties, the birefringence of OPCF is very sensitive to the structure.

In this letter, we numerically explore the possibility of designing a highly phase birefringent OPCF. Simulation results show that the phase birefringence of the OPCF is 3.43×10^{-2} at the wavelength of 1 550 nm. To the best of our knowledge, this is the first theoretical demonstration of such high level of phase birefringence for microstructured optical fibers. Due to the abovementioned properties, the proposed OPCFs in this letter have many optical applications in future.

The cross-section of the proposed OPCF is shown in Fig. 1. The cladding consists of an octagonal lattice with circular airholes in fused silica. The diameters of the first-ring airholes and the outer-ring airholes are d_1 and d_2, respectively. In order to obtain high birefringence, a rectangular array of four elliptical airholes was introduced in the core region. These holes were identical, with their diameters along the x- and y-axis denoted as a and b, respectively. The pitched between the holes in the vertical and horizontal directions were labeled as Λ_1 and Λ_2, respectively.

Due to the high refractive index contrast and complex structure, it is very difficult to obtain the simulation results for PCFs. Many modeling techniques have been applied in their characterization, including the finite element methods (FEMs)[21,22], plane-wave expansion method[23,24], finite difference time domain method[25], and multipole method[26]. In this letter, FEM with anisotropic perfectly matched layer (PML)[27] boundaries were used to calculate the modal complex effective refractive index n_{eff} by solving an eigenvalue drawn from the following Maxwell equation with a magnetic field:

$$\nabla \times (\varepsilon_\gamma^{-1} \nabla \times \mathbf{h}) - k_0^2 \mu_\gamma \mathbf{h} = 0, \tag{1}$$

where $\mathbf{h}$ is the magnetic field; ε_γ and μ_γ are the relative

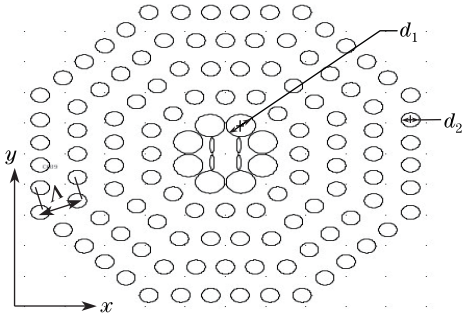

Fig. 1. Cross-section geometry of the proposed high birefringence OPCF.

dielectric permittivity and magnetic permeability complex tensors, respectively; k_0=$2\pi/\lambda$ is the wave number in the vacuum, and λ is the wavelength. The magnetic field of the modal solution is expressed as $\mathbf{h}$=$H\mathrm{e}^{-\gamma z}$, where H is the field distribution on the transverse plane, and $\gamma = \alpha$+jβ is the complex propagation constant with the attenuation constant α and the phase constant β. With the application of the variation finite element procedure, the above full vector equation yields the follow algebraic problem:

$$\mathbf{A} - \left(\frac{\gamma}{k_0}\right)^2 \mathbf{BH} = 0, \tag{2}$$

where the eigenvector $\mathbf{H}$ and the eigenvalue $(\gamma/k_0)^2$ provide the full vectorial magnetic field distribution and the effective index of the mode, respectively; $\mathbf{A}$ and $\mathbf{B}$ are symmetrical sparse matrices. We can get n_{eff} by solving Eq. (2). Then, the guiding properties of OPCFs, including phase birefringence $B(\lambda)$, chromatic dispersion D, confinement loss L and other properties, can readily be calculated. The material dispersion obtaining from the Sellmeier formula is included directly in our calculation.

Figure 2 shows the fundamental mode field profile of the proposed OPCF with the following parameters: Λ=2.0 μm, d_1=1.40 μm, d_2=0.92 μm, b=0.5 μm, Λ_1=0.6653×2 μm, Λ_2=0.5653×2 μm, and elliptical ratio a/b=0.1 at excitation wavelength λ=1 550 nm. The light was tightly confined in the high-index core region of proposed OPCF (Fig. 2). In addition, the y-polarized mode was stronger than the x-polarized model. The problem arises in part from the fact that y-polarized states have lower effective refractive indexes than that of x-polarized states.

Firstly, we numerically investigated the effect of the rectangular array of four elliptical airholes cladding in the OPCF core on the birefringence. Figure 3 shows the birefringence characteristics of the proposed OPCF versus wavelength at a/b values of 0.2, 0.4, 0.6, and 0.8, when b=0.5 μm. The three different airholes in the cladding were considered in our OPCF with the following parameters: Λ=2 μm, d_1=1.4 μm, d_2=0.92 μm, b=0.5 μm, Λ_1=0.6653×2 μm, and Λ_2= 0.5653×2 μm. As expected, the modal birefringence increased when the wavelength increased. Furthermore, the birefringence also increased with the increase of a/b, while the increasing speed of the birefringence decreased as the wavelength increased. When the value of a/b was less than 0.6, the increasing pace of birefringence in the long wavelength was fast. However, once the value of a/b was over 0.6, the max birefringence point trended to the short wavelength. The birefringence values for different a/b values of 0.2, 0.4, 0.6, and 0.8, were 1.65×10^{-2}, 2.32×10^{-2}, 2.98×10^{-2}, and 3.36×10^{-2}, respectively, at a wavelength of 1 550 nm. According to these results, the maximum birefringence increased by up to 3.36×10^{-2} at the wavelength of 1 550 nm when a/b was 0.8. The birefringence of 3.36×10^{-2} was two orders of magnitude higher than that of the traditional polarization maintaining optical fiber, and higher than the birefringence reported in Refs. [10,11,13]. This result offers the essential information for the characterization and the design of highly birefringent OPCF. We then kept the parameters Λ=2.0 μm, d_2=0.92 μm, a=0.4 μm, b=0.5 μm, Λ_1=0.6653×2 μm and Λ_2=0.5653×2 μm unchanged and changed d_1 of the first ring airholes from 1.42 to 1.46 μm with steps of 0.02. The result is shown in Fig. 4. By changing the diameter of the first ring airholes while keeping the other parameters unchanged, the birefringence in the short wavelength range was not obviously altered (Fig. 4). However, the value of the birefringence within the longer wavelength band increased with the enlargement of the diameters of the first ring airholes. The maximal birefringence value was 3.43×10^{-2} at a wavelength of 1 550 nm. To the best of our knowledge, this is a very high theoretical value at the communication wavelength in the field of microstructured optical fibers. In addition, according to the above analysis, the rectangular arrays of four elliptical airholes were mainly responsible for birefringence management. However, the diameters of the first ring airholes have little impact on the birefringence tailoring.

Chromatic dispersion in PCFs plays an important role

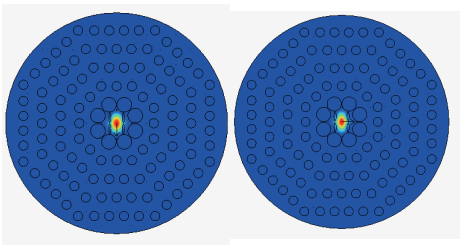

Fig. 2. Polarized mode field pattern of the HE_{11}^{y} (left) and HE_{11}^{x} (right) modes.

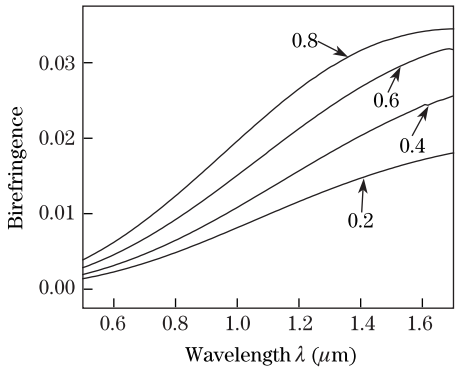

Fig. 3. Birefringence of the OPCF versus λ for four different a/b values (0.2, 0.4, 0.6, and 0.8; b=0.5 μm).

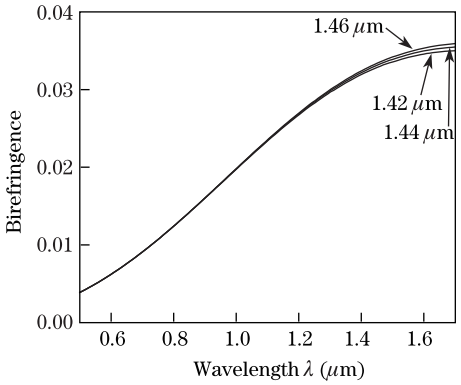

Fig. 4. Birefringence of the OPCF versus wavelength for three different d_1 values (1.42, 1.44, and 1.46 μm).

in optical communication as it limits the information carrying capacity of the fiber. In addition, the modal chromatic dispersion of the proposed OPCF changed in the HE_{11}^{y} and HE_{11}^{x} modes along with the wavelength when the parameters were unchanged (Λ=2.0 μm, d_2=0.92 μm, b=0.5 μm, Λ_2= 0.5653×2 μm, and Λ_1=0.6653×2 μm) for four different a/b values (0.2, 0.4, 0.6, and 0.8) (Figs. 5(a) and (b)). As seen from the same figures, the variation trend of the modal chromatic dispersion of the HE_{11}^{y} and HE_{11}^{x} modes was irregular. The zero dispersion wavelength (ZDW) shifted toward to the visible wavelength region as a/b increased. However, the minimal point of chromatic dispersion shifted toward the long wavelength. Moreover, the dispersion within the long wavelength region increased when the wavelength increased as the value of a/b became 0.2 for the HE_{11}^{y} mode, while the variation of modal dispersion of HE_{11}^{x} mode showed the opposite. The minimal dispersion value was –597 ps/(nm·km) at the wavelength of 1 550 nm. Then, we left the parameters (Λ=2.0 μm, d_2=0.92 μm, a=0.4 μm, b=0.5 μm, Λ_1=0.6653×2 μm, and Λ_2= 0.5653×2 μm) unchanged and changed the diameter d_1 of the first ring airholes from 1.42 to 1.46 μm with steps of 0.02 (Fig. 5(c)). Two ZDWs at 615 and 921 nm, respectively, were achieved using the proposed OPCF for the HE_{11}^{x} mode (Fig. 5(c)). The first ZDW was in the visible region, while the second ZDW was located in the working wave band of the Ti:sapphire oscillator (700–980 nm) which contributed to frequency conversion of Ti:sapphire femtosecond laser. PCF with two ZDWs can make strong power supercontiuum spectral in the near infrared band. However, there were no ZDWs for the HE_{11}^{y} mode in the proposed OPCF when the diameter d_1 of the first ring airholes changed from 1.42 to 1.46 μm with steps of 0.02. All values of dispersion showed negative values. According to our analysis, the rectangular arrays of four elliptical airholes made a slit for the HE_{11}^{y} mode waveguide, thus affecting the dispersion of the HE_{11}^{y} mode. As a result, there were no ZDWs for the HE_{11}^{y} polarization mode. Moreover, as can also be seen from the graph, the dispersion did not change with the change of the diameter of the first ring airholes for both the HE_{11}^{y} and HE_{11}^{x} modes. According to the analysis, the rectangular arrays of four elliptical

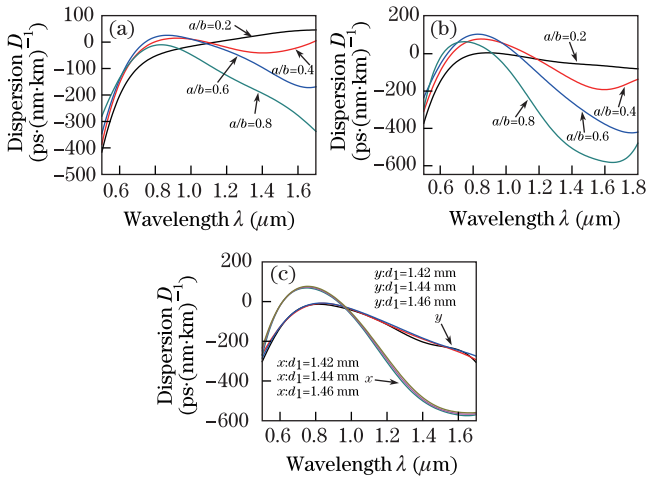

Fig. 5. Chromatic dispersion of the y axis and the x axis of the proposed OPCF.

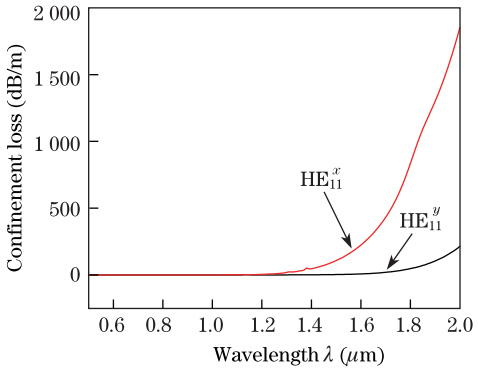

Fig. 6. Confinement loss as a function of the wavelength λ in the proposed OPCF.

airholes were mainly for dispersion management; however, the large airholes of the first ring in the outer cladding have little impact on the dispersion tailoring.

Figure 6 shows confinement loss of the HE_{11}^{y} and HE_{11}^{x} modes as the function of the wavelength. As expected, the losses increased with the wavelength because the field confinement decreased. The confinement loss of HE_{11}^{x} mode increased much faster than that of the HE_{11}^{y} mode in the long wavelength range. In addition, the magnitude of confinement loss of HE_{11}^{x} mode was so much higher than that of the HE_{11}^{y} mode. This property makes it possible to realize the single polarization single mode (SPSM) in our proposed OPCF.

In conclusion, a highly birefringent OPCF with a rectangular array of four elliptical airholes in the fiber core region has been successfully demonstrated through a modal solver based on FEM. Results show that our proposed OPCF shows a very high birefringence. The value of the phase birefringence increased by up to 3.43×10^{-2} at the wavelength 1 550 nm. The birefringence of 3.43×10^{-2} is two orders of magnitude higher than that of the traditional polarization maintaining fiber, and even higher than the birefringence reported in other references. Moreover, two ZDWs have been achieved using the proposed OPCF for HE_{11}^{x} mode. The first ZDW is in the visible region, however, the second ZDW is in the working wave band of the Ti:sapphire oscillator (700–980 nm), which contributes to the frequency conversion of Ti:sapphire femtosecond laser. It is expected that the proposed OPCF can be used as high birefringence and SPSM fiber.

This work was supported by the National Natural Science Foundation of China (No. 60637010) and the State Major Basic Research Development Program of China (No. 2010CB327604).

References

1. J. C. Knight, T. A. Birks, P. St. J. Russell, and D. M. Atkin, Opt. Lett. **21,** 1547 (1996).
2. J. C. Knight, Nature **424,** 847 (2003).
3. P. St. J. Russell, Science **229,** 358 (2003).
4. S. M. Abdur Razzak, Y. Namihira, K. Miyagi, F. Begum, S. Kaijage, N. H. Hai, T. Kinjo, and N. Zou, Opt. Rev. **14,** 14 (2007).
5. K. Saitoh, N. Florous, and M. Koshiba, Opt. Express **13,** 8365 (2005).

6. Y. Ni, L. An, Y. Xie, L. Zhang, and J. Peng, Opt. Commun. **235,** 305 (2004).
7. M. N. Hossain, M. S. Alam, D. Md. N. Hasan, and K. M. Mohsin, Photon. Lett. Poland **2,** 143 (2010).
8. A. Ortigosa-Blanch, J. C. Knight, W. J. Wadsworth, J. Arriaga, B. J. Mangan, T. A. Birks, and P. St. J. Russell, Opt. Lett. **25,** 1325 (2000).
9. T. P. Hansen, J. Broeng, S. E. B. Libori, E. Knudsen, A. Bjarklev, J. R. Jensen, and H. Simonsen, IEEE Photon. Technol. Lett. **13,** 588 (2001).
10. H. Xuan, J. Ju, and W. Jin, Opt. Express **18,** 3828 (2010).
11. Y. F. Chau, H. H. Yeh, and D. P. Tsai, Jpn. J. Appl. Phys. **46,** L1048 (2007).
12. Y. S. Sun, Y. F. Chau, H. H. Yeh, and D. P. Tsai, Jpn. J. Appl. Phys. **47,** 3755 (2008).
13. H. Zhou, S. Li, B. Fu, Y. Yao, and L. Zhang, Chin. Phys. Lett. **27,** 014208 (2010).
14. O. Frazao, in *Proccedings of 3rd WSEAS International Conference on Sensors, Signals and Materials* 155 (2010).
15. X. Ma and Y. Zhu, Chin. Opt. Lett. **8,** 983 (2010).
16. Z. He, Chin. Opt. Lett. **7,** 387 (2009).
17. L. An, Z. Zheng, Z. Li, T. Zhou, and J. Cheng, J. Lightwave Technol. **27,** 3175 (2009).
18. X. Chen, M. J. Li, N. Venkataraman, M. T. Gallagher, W. A. Wood, A. M. Crowley, J. P. Carberry, L. A. Zenteno, and K. W. Koch, Opt. Express **12,** 3888 (2004).
19. J. S. Chiang and T. L. Wu, Opt. Commun. **258,** 170 (2006).
20. S. M. A. Razzak and Y. Namihira, J. Light Electron. Opt. **122,** 1084 (2010).
21. S. Selleri, L. Vincetti, A. Cucinotta, and M. Zoboli, Opt. Quant. Electron. **33,** 359 (2001).
22. H. Zhang, B. Yang, Y. Liu, Q. Wang, L. Yu, and X. Zhang, Chin. Phys. B **18,** 1116 (2009).
23. S. Shi, C. Chen, and D. W. Prather, J. Opt. Soc. Am. A **21,** 1769 (2004).
24. Aaron J. Danner, "An introduction to the plane wave expansion method for caculating photonic crystal band diagrams", http://www.ece.nus.edu.sg/stfpage/eleadj/planewave.htm (January 31, 2011)
25. S. Lou, Z. Wang, G. Ren, and S. Jian, Opt. Fiber Technol. **11,** 34 (2005).
26. T. P. White, B. T. Kuhlmey, R. C. McPhedran, D. Maystre, G. Renversez, C. M. D. Sterke, and L. C. Botten, J. Opt. Soc. Am. B **19,** 2322 (2002).
27. K. Saitoh and M. Koshiba, J. Lightwave Technol. **19,** 405 (2001).